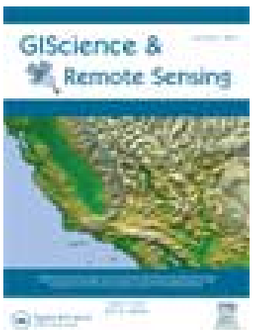

GIScience & Remote Sensing

ISSN: 1548-1603 (Print) 1943-7226 (Online) Journal homepage: http://www.tandfonline.com/loi/tgrs20

First order approximation of Broadband Directional Albedo with High Resolution Quickbird Imagery: a case study for arid urban areas.

Shai Kaplan, Christopher S. Galletti, Winston T.L. Chow & Soe W. Myint

To cite this article: Shai Kaplan, Christopher S. Galletti, Winston T.L. Chow & Soe W. Myint (2016): First order approximation of Broadband Directional Albedo with High Resolution Quickbird Imagery: a case study for arid urban areas., GIScience & Remote Sensing, DOI: 10.1080/15481603.2016.1153944

To link to this article: http://dx.doi.org/10.1080/15481603.2016.1153944

Publisher: Taylor & Francis

Journal: *GIScience & Remote Sensing*

DOI: 10.1080/15481603.2016.1153944

First order approximation of Broadband Directional Albedo with High Resolution Quickbird Imagery: a case study for arid urban areas.

Shai Kaplan[1],

The Jacob Blaustein Institute for Desert Research, Ben-Gurion University of the Negev, Israel

Christopher S. Galletti

School of Geographical Sciences and Urban Planning, Arizona State University, Tempe, AZ., United States of America

Winston T.L. Chow

Department of Geography, National University of Singapore, Kent Ridge, Singapore

Soe W. Myint

School of Geographical Sciences and Urban Planning, Arizona State University, Tempe, AZ., United States of America

Submitted to GIScience & Remote Sensing on May 26, 2015

[1] skaplan3@asu.edu

Abstract

Albedo is a key forcing parameter controlling the planetary radiative energy budget and its partitioning between the surface and the atmosphere. Characterizing and developing high resolution albedo for an urban environment in arid regions is important because of the high urbanization rate in these regions and because of the high land-cover heterogeneity within urban settings. Using a Monte-Carlo simulation of a multi-variable regression, we (a) correlate directional solar reflectance (albedo) ground measurements from Phoenix, AZ, with four narrowband reflectance data from QuickBird, and (b) developed a new set of coefficients for converting QuickBird narrowband reflectances to albedo. The albedo models were then applied to a second image over Las Vegas, NV, to assess their feasibility and accuracy. Two wavebands, visible-near infrared (VNIR) and total shortwave albedo, were evaluated for two reflectance models: surface and top-of-atmosphere. Results show that it is possible to accurately estimate directional albedo from high resolution imagery, specifically QuickBird, with the most accurate result from an atmospherically corrected VNIR model. The methodology presented in this paper could thus be applied in other urban areas to obtain a first order estimation of albedo. The new set of coefficients can be applied as first order albedo estimate by researchers, urban planners, developers and city managers interested in the influence of high-resolution albedo on a myriad of urban ecosystem processes.

Keywords: albedo, urban, Quickbird, modeling, arid regions, high resolution

I. Introduction

Land surface broadband albedo is a critical component that impacts Earth's climate and provides an indicator of environmental vulnerability. Albedo is defined as the ratio of the radiant solar flux reflected from the Earth's surface to the downward solar flux. It is a key forcing parameter controlling the planetary radiative energy budget and its partitioning between the surface and atmosphere. Albedo has high spatial and temporal variability resulting from both natural processes (e.g. solar illumination, snowfall and vegetation growth) and human activities (e.g. built environment, vegetation clearing and agricultural practices) (Liang 2001). In arid and semi-arid environments, where water is the most critical resource, changes in surface processes as a result of increased albedo may inhibit a negative feedback cycle on precipitation (GCOS 2004).

Calculations of directional albedo are essentially an integral estimated from spectral reflectance, between wavelengths λ_x and λ_y. The calculation of the broadband albedo - α (Equation 1 and 2) then follows from Liang (2000) and can be estimated from the spectral reflectance measured at a surface (Liang, Strahler and Walthall, 1999):

$$\alpha_\Lambda = \int_{\lambda_x}^{\lambda_y} r\,(\lambda)\mathrm{d}\lambda \qquad (1)$$

and,

$$r = \frac{f_u\,(\Lambda)}{f_d(\Lambda)} \qquad (2)$$

where Λ is the waveband between wavelengths λ_x and λ_y, f_u and f_d are the upwelling and downwelling radiative fluxes, respectively, as measured using instruments, and r is the spectral reflectance between wavelengths λ_x and λ_y (i.e. spectral signature)

One area where albedo is important for moderating ecosystem properties is urban environments. In recent decades, many of the world's arid and semi-arid environments have experienced high rates of urbanization. Urbanization is considered one of the most intensive land transformation processes: it

incorporates a wide range of land cover and land use types associated with the built environment where albedo can have variable multi-scale effects, as it alters natural biophysical processes including local surface energy balance (Grimm et al. 2008; Imhoff et al. 2000). Altering the surface energy balance influences climate across scales: from micro-climate implications on human comfort and irrigation to energy use, air quality and the development of the urban heat island (UHI) phenomenon (Oke 1987) at the city and regional scale (Rose and Levinson, 2013). For instance, urban surface albedo modification through "white roofs" and "green roofs" is a viable technique that can mitigate the UHI at the building or neighborhood scale (Taha, 1997; Georgescu, Mahalov and Moustaoui 2012). Regional (i.e. city-wide) increases in albedo that have been simulated through prognostic climate models show that white roofs can significantly lower urban-induced warming, but may potentially affect other climate processes such as reduced precipitation at regional (Georgescu, Mahalov and Moustaoui, 2012; Georgescu et al. 2013) and continental scales (Georgescu et al. 2014). On a global scale, increasing world-wide albedos of urban roofs and paved surfaces by 0.1 has been modeled and results show a potential net negative radiative forcing on the Earth equivalent to offsetting about 44 Gt of CO^2 emissions (Akbari and Matthews, 2012). Understanding fine scale changes in albedo can offer new insights into how this ecosystem property can be managed sustainably. Moreover, arid land natural landscapes are typically characterized by high albedo compare to the low albedo typically observed for urban areas; thus the impacts of changes in albedo due to urbanization will be manifested more intensely and rapidly.

Remote sensing is the only feasible method for continuous monitoring and measurement of surface albedo over large areas. Liang (2001) developed conversion formulas for a series of satellite sensors that correlate albedo to land covers. The crux of the conversion formula, from satellite spectral measurements to albedo, is a set of coefficients that relate the sensor's individual bands to simulated hemispherical broadband albedo. These conversion formulas are still used today for a wide range of sensors, such as the Advanced Spaceborne Thermal Emission and Reflection Radiometer (ASTER), Advanced Very High Resolution Radiometer (AVHRR), Landsat ETM+/TM, and Moderate Resolution Imaging Spectroradiometer (MODIS). However, the above mentioned sensors are mostly low and

medium resolution sensors which are not suitable to monitor highly heterogenic landscape such as urban environments.

Urban land covers vary greatly over small distances. High resolution satellite imagery is increasingly used to observe, monitor and validate land change processes and biophysical characteristics of urban environments, (e.g. Li et al. 2013; Myint et al. 2010). To date, there has been little work in relating broadband albedo to the multispectral data from high resolution sensors, mostly because the focus of previous albedo measurements have been at larger scales where medium or low resolution imagery is sufficient and high resolution images can be costly or not available. Recently, Ban-Weiss et al. (2013) used multiband aerial imagery to derive the albedos of individual roofs in California. Rose and Levinson (2013) manually digitized high resolution ortho-photo combined with Lidar data and hillshade analysis to evaluate the effect of tree shading on albedo in residential areas. Our aim is to assess whether it is feasible to use high resolution imagery to model directional albedo for multiple land cover types, and to develop a conversion formulas that can be applied to QuickBird images over urban arid environments. The study uses an empirical approach that can be applied independently using only image and field data to derive first order estimates of albedo at high resolution. While this technique is similar to previous work by Liang (2000; 2002)) and Ban-Weiss et al. (2013), the advantage of our methodology is that it directly correlates ground-based observations with satellite-based observations without the need for extensive computing or simulation, and consider all land-cover types

II. Study area and Data

To understand the human impact of albedo in urban environments, especially in arid and semi-arid environments, we developed empirical relationships between high resolution QuickBird broadband reflectances and directional albedo derived from ground narrowband measurements using multivariate regression. The ground directional albedos were measured during a field campaign in Phoenix, Arizona, USA, and the high resolution data were collected from a QuickBird flyover during the week of our fieldwork. A new set of coefficients was developed to estimate albedo directly from image data. The new

coefficients were then applied to a second QuickBird image taken over Las Vegas, Nevada, USA and the resulting albedo values were compared against ground measurements carried out in Las Vegas.

A. Study area

Two areas were considered for this study - Phoenix, Arizona and Las Vegas, Nevada (Figure 1). The image acquired over Phoenix was used to develop the model and the Las Vegas image was used for validation. Both cities are located in the same Köppen-Geiger climate zone (*BWh*), and both have experienced rapid urbanization since the 1960's. In Phoenix much of the urban expansion is characterized by the replacement of agricultural or open desert areas with residential and commercial/industrial land uses. A similar land-use and land cover change occurred in Las Vegas with mostly residential expansion into adjacent shrubland desert and fluvial pans. Currently, the urban area of Phoenix metropolitan area is ~ 3000 km^2 with population of ~4.49 million (U.S. Census 2010); The urban area of Las-Vegas is ~352 km^2 with population of ~585,000. Combined with an arid climate, the urban expansion in both cities has induced a suite of human environment problems that include a large UHI and alteration of many ecosystem services (Gober 2006; Chow et al. 2012). With the large number of cloud-free days per year resulting in substantial fluxes of solar energy either being absorbed or reflected by the various land covers of the city, intra-urban albedo variations are potentially important in UHI development and has a strong impact on micro-climate regulation in these desert cities. With the large intra-urban variability of land-use and land cover (Buyantuyev and Wu 2010; Myint and Okin 2009), high resolution satellite imagery is one of the most appropriate tools for studying biophysical phenomena within the urban environment whenever available.

B. Imagery

Two QuickBird multispectral images with four bands (450–520 nm, 520–600 nm, 630–690 nm, and 760–900 nm) at a 2.44-m were acquired: the first over Phoenix on July 11th, 2012, at 10:40 h local time, and a second over Las Vegas on September 2nd, 2012, at 10:57 h local time. The former was used to develop the model, and the latter was used for its validation. Table 1 shows images and climate characteristics at the time of acquisition. Because the QuickBird data (along with many other high

resolution sensors) covers the visible and NIR portion of the spectrum, the goal and challenge of modeling broadband albedo with high resolution sensors is to try and develop a viable model that can accurately estimate albedo across the total shortwave band (i.e. the visible and reflected infrared part of the spectrum – 320-2500nm).

The training image is comprised of a 5 by 5 km area of West Phoenix (Figure 2a). This area was chosen because it includes a multitude of land use (e.g. residential, commercial, industrial, and agricultural) and land cover types (e.g. buildings, open soil, trees and shrubs, grasses, pools, impervious surfaces, and water). A micrometeorological tower (WPHX; Figure 2c) (Chow et al. 2014) that conducts eddy covariance measurements at 22.3 m (73 ft) a.g.l. is also located within the study area. A mean mid-day value of surface albedo was subsequently derived from the pyranometer components of the all-wave net radiometer (Hukseflux NR01) installed *in situ*. Based on the instrument height and sensor field-of-view (Oke 2006), we estimated a circular source area for radiation (and albedo) measurements of radius 230 m that was centered at the WPHX site (Figure 2c).

➔ Fig. 1.

➔ Fig. 2.

Due to the differences in spectral range between the pyranometer and QuickBird, we also used an image taken by the airborne MODIS/ASTER Simulator, or MASTER, instrument for validation (Figure 2b). The MASTER sensor acquires data over the visible through mid-infrared wavelengths (0.46 – 12.817 μm) in 50 spectral bands (Hook et al. 2001), at approximately 7 m/pixel. The data were acquired during July 2011, as part of a data collection campaign over Phoenix (See Jenerette et al. 2015). The overlapping area between the Quickbird image and the MASTER data is shown in figure 2a.

C. Albedo ground measurements

Ground spectral measurements were taken near the QuickBird overpass time under similar weather conditions. The spectral readings were taken using an ASD FieldSpec-4 Wide-Res spectrometer that measures reflectance at the visible and NIR wavelength range (350-2500 nm). In Phoenix, a total of 71 samples were collected from various sites within the image boundaries. In Las Vegas, 40 samples were

collected. The reflectance of each sample was measured 4 times, at 5-15 cm above the sample surface/canopy. The final spectral signature for each sample was derived by averaging the 4 measurements.

We collected spectral measurement samples from both cities, which were taken over the land-use and land cover types listed in the preceding section. Figure 3 shows the final spectral signature for the dominant land cover types collected. Land cover types include soil, impervious surfaces, vegetation, and several different types of roof tops. These represent the main urban features typical for the Phoenix and Las Vegas metropolitan areas, and were considered critical for the estimation of broadband albedo in urban areas.

A Garmin eTrex Global Positioning System (GPS) unit with accuracy of <3m, was used to mark the locations of spectrometer samples from the field. These spectrometer readings were then georeferenced in ArcGIS for comparison with the QuickBird image.

➔ Fig. 3.

III. Methods

Our paper uses an empirical approach that can be applied independently using only image and field data to derive first order directional albedo estimates at high resolution.

A. Conversion to reflectance

Liang et al. (2003) indicated there are two important pre-processing steps when estimating albedo: (1) radiometric calibration of the sensor - converting digital numbers (DNs) to top-of-atmosphere (TOA) radiance and then to TOA reflectance; and (2) conversion of the TOA reflectance to surface reflectance. The raw image data were converted to TOA radiance and then to TOA reflectance following Krause (2005). To calibrate TOA reflectance to surface reflectance we used the FLAASH module in ENVI 4.8 software (http://www.exelisvis.com/docs/FLAASH.html). The FLAASH incorporates the MODTRAN4 radiation transfer code, and is a first principle atmospheric correction tool. Within the FLAASH module - mid-latitude summer atmospheric model and urban aerosol model were used for both

images. Past studies have validated FLAASH by comparing to ground reflectance measurements and found that the FLAASH-corrected spectra were the same as the ground-collected spectra within the uncertainty of the ground truth measurements (Berk et al. 1998; Matthew et al. 2000). To further assess the atmospheric correction, we compared the FLAASH corrected image spectral reflectance to the ground spectra of various land-cover types (soil, grass, desert shrub, tree, concrete, water, and asphalt road) collected at the time of the sensor's overpass (Figure 4). We used the QuickBird spectral response function to re-sample the ground spectra in order to match wavelengths and band-width, i.e. each wavelength of the ASD spectrometer was multiplied by the QuickBird sensor efficiency (%). Our assessment indicate that there is excellent agreement between the atmospherically corrected image reflectance and the ground spectra (R^2=0.99, RMSE=0.02).

➔ Fig. 4.

The TOA and surface reflectance were imported into ArcGIS along with the broadband directional albedos measured in the field. Together, the field measurements of the empirical broadband directional albedo and the two reflectance models from QuickBird served as the data for our regression analysis.

The MASTER data were converted to reflectance using the quick atmospheric correction (QUAC) algorithm (Bernstein et al. 2005) within ENVI/IDL (version4.8). The image was georeferenced to align with the Phoenix QuickBird image, with a target registration error of no more than 0.5 pixels. Albedo was estimated using the empirical formula previously developed for the MODIS sensor (Liang 2001; Equation 3):

$$\alpha_{vis} = 0.331\alpha5 + 0.424\alpha1 + 0.246\alpha3 \quad (3)$$

where α1, α3, and α5 are reflectances in MASTER spectral channels 1 (0.46 μm), 3 (0.54 μm), and 5 (0.66 μm), respectively.

B. Ground albedo

As a first order empirical observation of albedo we calculate the directional albedo from surface solar reflectance measurements of various urban land cover types. The field measurements were taken using a portable spectrometer (see data section above for more instrumental details). We considered two broad wavebands: the visible and near infrared, or α_{vnir} (450-900 nm), and the total solar reflectance, or α_{TOT} (350-2320 nm). The reason that we adopted the first is because it corresponds to the satellite spectral range. The second was adopted because downward fluxes beyond this range are very small, thus their contribution to albedo is negligible. Overall, the visible and NIR corresponds to approximately 90% of the solar spectrum that reaches the Earth's surface (Prado and Ferreira, 2005). We estimated the directional albedo at the surface by taking the integral of spectral reflectance measurements in the field with a portable spectrometer (equation 1).

C. Linear Modeling

To develop the models and calibrate its coefficients we employed an ordinary least squares (OLS) approach. OLS assumes a linear relationship between the dependent variable - the empirical broadband directional albedo as measured in the field with our portable spectrometer, and the independent variables - the reflectance values for the blue, green, red, and NIR bands of the QuickBird image. We implemented a backward elimination regression process to automatically prune the most significant variables from the four possible QuickBird bands and adjust the coefficients. The backward elimination regression is akin to a data mining technique that selects the most significant variables for prediction. The selection process in the backward elimination started with all four QuickBird bands in the model and then eliminated a single variable with the least significant correlation to the dependent variable. An assessment of the F value is performed to consider possible inclusion back into the model (IBM 2011). If the variable does not meet the default criteria for the F value test (0.1 significance) then the model is accepted and the coefficients are updated and the process begins again. Four sets of coefficients were considered:

(1) $\alpha_{TOT\text{-}TOA}$ - total shortwave directional albedo for top of atmosphere reflectance;

(2) $\alpha_{TOT\text{-}SURF}$ - total shortwave directional albedo for surface reflectance

(3) $\alpha_{VNIR\text{-}TOA}$ - VNIR shortwave directional albedo for top of atmosphere reflectance;

(4) $\alpha_{VNIR\text{-}SURF}$ - VNIR shortwave directional albedo for surface reflectance.

Finally, to fine-tune the model after the backward elimination process, we applied a Monte Carlo-like simulation on the final variables for each model. The process was conducted in the 'R' software environment and used the ordinary linear model function to calculate a least-squares regression over a large number of iterations. In each iteration 15% of the observations were excluded from the regression process. 10,000 iterations were performed and the mean of all the iterations was recorded as the new coefficient for each variable. In all cases this resulted in only a slight change in the coefficients. The R^2 of the final model was calculated using methods common for regression through the origin (Eisenhauer 2003).

The coefficients were evaluated by the R^2 produced from the multiple regression models, as well as compared to a pyranometer that is part of a micrometeorological tower conducting eddy covariance measurements located within the Phoenix study area. Finally, the coefficients of the best statistical model were applied to the second QuickBird image taken over Las Vegas. The resulting albedo image values were compared to ground measurements (i.e. – spectral albedo measured with the portable spectrometer).

IV. Results and Discussion

I. Conversion formulas

The following are the formulas for converting surface narrow-band albedos to two broadband albedos: VNIR: 0.4-0.9µm, and; total shortwave (TOT): 0.35-2.32µm, based on the multiple regression and the Monte-Carlo procedures reported earlier for TOA and surface reflectance (surf):

$$\alpha_{VNIR-TOA} = -1.039b_1 + 1.718b_2 + 0.281b_4$$

$$\alpha_{VNIR-surf} = 0.546b_2 + 0.431b_4$$

$$\alpha_{\mathrm{TOT-TOA}} = -0.248b_1 + 0.739b_3 + 0.378b_4$$

$$\alpha_{\mathrm{TOT-surf}} = 0.428b_3 + 0.491b_4$$

Where b_x is the reflectance of QuickBird band *x*.

The coefficients have been developed using 70 samples. Results show that the NIR band is used in all models, most likely due to its high reflectance values on most land covers (in both image and field measurements). Two differences were noted. First, the blue band is eliminated in the surface reflectance models. This is probably due to the fact that the blue band is the wavelength with the highest relative scatter (Rayleigh scattering) and is being corrected the most for atmospheric effects (Chavez 1996; Sabins 2007). Second, while the α_{vnir} models uses b_2 (green band) as a significant band, the α_{tot} models replace b_2 with b_3 (red band). Both of these bands are in the visible range of the spectrum and have been shown to be highly correlated. Figure 5 shows the final broadband albedo estimations of the Phoenix area.

➔ Fig. 5.

B. Model evaluation and implications

The challenge of creating a broadband albedo model is in determining the accuracy of the coefficients that are applied to the reflectance values of each band. We used two primary indicators to evaluate the retrieval model for the PHX image: the R^2 of the regression model and the broadband albedo as measured by a pyranometer located at WPHX. It is important to note that the pyranometer integrates across the viewing hemisphere and provides a "landscape-level" estimate. The ground measurements and the high resolution imagery provide a snapshot of the land surface with a specific viewing angle, usually referred to as directional/instantaneous albedo. Comparing remote sensing models to albedo measured at a pyranometer provides a way to understand and evaluate how well we can model albedo from satellite imagery.

For comparison with WPHX, we applied the coefficients from all four models to the pixels within the estimated pyranometer source area. We measured the mean broadband albedo calculated for all pixels and compared that with the measured albedo for the same day and within 10 minutes of the image capture

time by the QuickBird satellite. Regression analysis shows that all models are in high agreement with the flux tower observations with R^2>0.93 (Table 2). However, all models show overestimation ranging 2.3 to 6.7% compared to the pyranometer measurements (Table 2). Liu et al. (2009) concluded that site heterogeneity and spatial scale can lead to discrepancies between ground-measured albedo and remote sensing albedo estimates. Thus, the overestimation could be attributed to the difference between the pyranometer's hemispherical integrated albedo and the directional albedo estimated by our models. The smallest differences between the broadband albedo estimates and that measured by WPHX came from the surface VNIR model. The surface-VNIR model estimated albedo to be 0.191 compared to 0.168 measured by the pyranometer. Statistical analyses indicated all models have small RMS (<0.008), and that surface models show a positive bias whereas TOA models show smaller negative bias. We believe this reveals some possible bias inherent in the atmospheric correction. Whether this is due to the method used or some other factor remains an open question for future study that will investigate using radiative transfer models (Liang 2001).

The relationship between the ground measured albedo and the predicted albedo for the four models produced is depicted in Figure 6. All models show high accuracy with R^2 ranging 0.83 to 0.86. As expected, surface models prediction is closer to the 1:1 slope compared to TOA models. Following Liang (2000), it demonstrates the importance of the atmospheric correction as the TOA models underestimate albedo, whereas the atmospherically corrected models are closer to the 1:1 line with a slight overestimation (<2.3%).

➔ Table 2

➔ Fig. 6.

Using the new set of coefficients, we generated high resolution broadband albedo maps from QuickBird data. Figure 5 illustrates the broadband albedo maps using the best two models, i.e. VNIR/Surface and TOT/Surface. Visually, the spatial pattern and magnitude of both look reasonable, and follows general land cover properties. For example, large industrial/commercial buildings with white roof tops show high albedo and parking lots and asphalt roads show low albedo. To further evaluate the

model's accuracy, albedo estimates form the VNIR/Surface model, were compared to albedo estimates derived from the atmospherically corrected MASTER sensor (Figure 7). Regression analysis indicates a strong relationship with R^2=0.84 and RMSE=0.04. The main difference was observed for high albedo features (albedo>0.4), where our VNIR/Surface model underestimates albedo compare to the values derived from the MASTER data.

➔ Fig. 7.

To provide additional information on the estimation accuracy, the two best derived models were applied to the image taken over Las Vegas. As in the Phoenix image, albedo values follow the general land cover pattern. Figure 8 shows the original Las Vegas image with field site locations, and the resulting albedo image produced by the best model (VNIR/Surface). The same statistical evaluation was applied for estimating accuracy of the model (Table 3).

➔ Fig. 8.

➔ Table 3.

Results show that the values over Las Vegas have slightly lower R^2 with higher bias and RMS compare to the Phoenix models. These differences could be attributed to small but distinct variations in climate and image characteristics between study areas (Table 1), such as from the different image timing (early summer in Phoenix vs. late summer in Las Vegas), difference in cloud cover conditions, or seasonal difference in surface moisture (e.g. monsoon). Regardless, the conversion formulas produce generally high accuracy and can be used to predict broadband albedo from Quickbird images over these urban environments.

Comparing the α_{tot} vs. α_{vnir} models, the α_{vnir} captures the total shortwave part of the spectrum more accurately. Nevertheless, both estimates are very similar. The reason for these close estimates, without the benefit of data points above the 900 nm wavelength, we believe, is that the QuickBird bands with three visible bands and one near-infrared band captures the critical portion of the spectrum where

most of the energy would be absorbed or reflected by the surface. Because this is where the bulk of the solar flux resides, we believe this indicates that albedo can be reasonably estimated using just the VNIR bands. There are two caveats to this though.

We must note certain limitations to our approach. First, the atmospheric correction is critical because it improves model performance. Second, for true surface energy balance models the albedo estimates will need to incorporate bidirectional reflectance more thoroughly. In our estimates, we take averages of reflectance at the ground (from a few slightly different angles). But in order for more accurate energy models, bidirectional estimates will need to be incorporated (Liang 2000). Third, we forgo weighted estimates of each band mainly because our measurements are based on satellite data with four bands from the visual and near infrared part of the spectrum, where most of the solar energy reaching the Earth's surface resides. Future research will incorporate both weighted estimates and integrate over observation angles to fine tune future albedo estimates. Until then and until more studies are completed, the generalizability of estimating the total shortwave albedo from VNIR coefficients is unknown. Nevertheless, it seems that high resolution imagery is capable of providing a first order estimate of albedo such as needed for microclimate studies.

V. Conclusions

We developed new coefficients for estimating and modeling broadband albedo from high resolution QuickBird images over arid environments. Unlike other studies, where albedo coefficients have been developed using semi-empirical simulations, our results are based on the empirical relationship between ground measurements and sensor data. The coefficients were developed using multiple regression, as well as a backward elimination procedure and Monte Carlo simulation for variable pruning and fine-tuning of the coefficients, respectively. The derived coefficients were validated by a micrometeorological tower located within the study area, a comparison to albedo values derived from airborne image using Liang (2001) furmula, as well as applied to a second image over a different city. The results indicate a high level of accuracy for both locations, suggesting they are robust despite

differences in climatic and image characteristics. Applying the methodology described herein to other images with different viewing and illumination geometry, over different urban areas, and during different seasons will allow further validation and sensitivity testing, as well as fine tuning and more generalization of the proposed coefficients.

Characterizing and developing high resolution albedo is especially important for urban environments because the physical processes and spectral characteristics occur at the scale of 10-20m (Small 2003). Our study shows that accurate broadband albedo models can be developed from high resolution imagery, which could be subsequently applied by urban ecosystem researchers, planners, and decision makers interested towards processes and policy outcomes related to surface energetics such as the UHI. This seems particularly so at the neighborhood or sub-city scale where albedo can play an important role in land surface temperatures, especially towards mitigating excessive urban warmth.

Acknowledgments

This work was supported by the School of Geographical Sciences and Urban Planning at Arizona State University and the National Science Foundation under Grant DEB-0423704, Central Arizona-Phoenix Long-Term Ecological Research (CAP LTER). Any opinions, findings, and conclusions or recommendations expressed in this material are those of the authors and do not necessarily reflect the views of the National Science Foundation. The study was conducted under the auspices of the Environmental Remote Sensing and Geoinformatics Lab. The authors thank Dr. Anthony J. Brazel for his advice and help in field data collection.

VI. References

Akbari, H. and H.D. Matthews (2012) "Global cooling updates: reflective roofs and pavements," *Energy and Buildings*, 55, 2-6, doi:10.1016/j.enbuild.2012.02.055.

American Society for Testing and Materials (ASTM) (2003) Reference Solar Spectral Irradiance: Air Mass 1.5 [online]. Available: http://rredc.nrel.gov/solar/spectra/am1.5/

Berk, A., L. S. Bernstein, G. P. Anderson, P. K. Acharya, D. C. Robertson, J.H. Chetwynd, and S. M. Adler-Golden, (1998) MODTRAN Cloud and Multiple Scattering Upgrades with Application to AVIRIS. Remote Sensing of the Environment, 65:367-375.

Buyantuyev, A., and J. Wu (2010) "Urban heat islands and landscape heterogeneity: linking spatiotemporal variations in surface temperatures to land-cover and socioeconomic patterns," *Landscape Ecology*, 25 (1), 17-33, doi:10.1007/s10980-009-9402-4.

Chavez, P.S. (1996) "Image-based atmospheric corrections - revisited and improved," *Photogrammetric Engineering & Remote Sensing*, 62 (9), 1025-1036.

Chow, W.T.L. D. Brennan, and A.J. Brazel (2012) "Urban heat island research in Phoenix, Arizona: theoretical contributions and policy applications," *Bulletin of the American. Meteorological Society*, 93 (4), 517–530, doi:10.1175/BAMS-D-11-00011.1.

Chow, W.T.L., T.J. Volo, E.R. Vivoni, G.D. Jenerette, and B.L. Ruddell (2014) "Seasonal dynamics of a suburban energy balance in Phoenix, Arizona" *International Journal of Climatology*. doi: 10.1002/joc.3947.

Eisenhauer, J.G. (2003) "Regression through the origin," *Teaching. Statistics*, 25 (3), 76-80, doi: 10.1111/1467-9639.00136.

Georgescu, M. A. Mahalov, and M. Moustaoui (2012) "Seasonal hydroclimatic impact of Sun Corridor expansion" *Environmental Research Letters*, 7 (3), 034026 doi:10.1088/1748-9326/7/3/034026.

Georgescu, M., M. Moustaoui, A. Mahalov, and J. Dudhia (2013) "Summer-time climate impacts of projected megapolitan expansion in Arizona," *Nature Climate Change,* 3, 37-41 doi: 10.1038/nclimate1656.

Georgescu, M. P.E. Morefield, B.G. Bierwagen, and C.P. Weaver (2014) " Urban adaptation can roll back warming of emerging megapolitan regions" *Proceedings of the National Academy of Sciences*, 111 (8), 2909-2914, doi: 10.1073/pnas.1322280111.

Global Climate Observing System (GCOS) (2004), Implementation plan for the Global Observing System for Climate in support of the UNFCCC. *Report GCOS – 92 (WMO/TD No.1219)*. [online]. 136p. Available: http://www.wmo.int/pages/prog/gcos/Publications/gcos-92_GIP_ES.pdf

Gober, P. (2006) *Metropolitan Phoenix: place making and community building in the desert*, Philadelphia: University of Pennsylvania Press.

Grimm, N.B., S.H. Faeth, N.E. Golubiewski, C.L. Redman, J. Wu, X. Bai, and J.M. Briggs (2008), "Global change and the ecology of cities," *Science,* 319 (5864), 756-760, doi:10.1126/science.1150195

Gueymard, C. (2004) "The sun's total and spectral irradiance for solar energy applications and solar radiation models," *Solar Energy*, 76 (4), 423-453, doi:10.1016/j.solener.2003.08.039.

Hook, S.J., Myers, J.E.J., Thome, K.J., Fitzgerald M., and Kahle, A.B. (2001) The MODIS/ASTER airborne simulator (MASTER)—a new instrument for earth science studies. *Remote Sensing of Environment* 76:93–102

IBM (2011), *IBM SPSS Statistics Version 20 Brief Guide.* 170 p.

Imhoff, M.L., C.J. Tucker, W.T. Lawrence, and D.C. Stutzer (2000) "The use of multisource satellite and geospatial data to study the effect of urbanization on primary productivity in the United States" *IEEE Transactions on Geoscience and Remote Sensing,* 38 (6), 2549-2556. doi: 10.1109/36.885202.

Jenerette, D.G., Harlan, S.L., Buyantuev, A., Stefanov, W.L., Declet-Barreto, J., Ruddell, B.L., Myint, S.W., Kaplan, S, and Li, X. (2015) "Micro-scale urban surface temperatures are related to land-

cover features and residential heat related health impacts in Phoenix, AZ USA," *Landscape Ecology*, DOI 10.1007/s10980-015-0284-3

Krause, K. (2005) *Radiometric Use of QuickBird Imagery,* Colorado: DigitalGlobe.

Li, G., Lu, D., Moran, E. and Hetrick ,S. (2013). Mapping impervious surface area in the Brazilian Amazon using Landsat Imagery. *GIScience and Remote Sensing*, 50, 172-183.

Liang, S.L. (2001), "Narrowband to broadband conversions of land surface albedo: I Algorithms," *Remote Sensing of Environment*, 76 (2), pp. 213-238, doi:10.1016/S0034-4257(00)00205-4

Liang, S.L. (2007) "Recent developments in estimating land surface biogeophysical variables from optical remote sensing," *Progress in Physical Geography*, 31 (5), 501–516, doi: 10.1177/0309133307084626.

Liang, S.L., A. Strahler, and C. Walthall (1999) "Retrieval of land surface albedo from satellite observations: a simulation study," *Journal of Applied Meteorology*, 38, 712-725. doi:10.1175/1520-0450(1999)038<0712:ROLSAF>2.0.CO;2

Liang, S.L., H. Fang, M. Kaul, T. Van Niel, T. McVicar, J. Pearlman, C. Walthall, C. Daughtry, and F. Huemmerich (2003) "Estimation and validation of land surface broadband albedos and leaf area index from EO-1 ALI data," *IEEE Transactions on Geoscience and Remote Sensing*, 41 (6), 1260-1267, doi:10.1109/TGRS.2003.813203.

Liu, J., Schaaf, C., Strahler, A., Jiao, Z., Shuai, Y., Zhang, Q., Roman, M., Augustine, J.A., and Dutton, E.G. (2009) " Validation of Moderate Resolution Imaging Spectroradiometer (MODIS) albedo retrieval algorithm: Depending of albedo on solar zenith angle," *Journal of Geophysical Research*, 114, D01106, doi:10.1029/2008JD009969.

Myint S.W., and G.S. Okin (2009), "Modelling land-cover types using multiple endmember spectral mixture analysis in a desert city," *International Journal of Remote Sensing*, 30 (9), 2237–2257, doi:10.1080/01431160802549328.

Myint, S.W., Brazel, A., Okin, G. and Buyantuyev, A. (2010) Combined Effects of Impervious Surface and Vegetation Cover on Air Temperature Variations in a Rapidly Expanding Desert City. *GIScience & Remote Sensing*, **47** (3), 301-320.

Oke, T.R. (1987) *Boundary Layer Climates*, 2nd ed., London: Methuen.

Oke, T. R. (2006) "Initial Guidance to Obtain Representative Meteorological Observations at Urban Sites," Instruments and Methods of Observation Program, IOM Report No. 81, WMO/TD 1250, Geneva: World Meteorological Organization, 2006. [online]. 81p. Available: http://www.urban-climate.org/documents/IOM-81-UrbanMetObs.pdf.

Pinty, B., T. Lavergne, T. Kaminski, O. Aussedat, R. Giering, N. Gobron, M. Taberner, M. M. Verstraete, M. Voßbeck, and J.-L. Widlowski (2008), Partitioning the solar radiant fluxes in forest canopies in the presence of snow, *Journal of Geophysical Research*, 113, D04104, doi:10.1029/2007JD009096.

Prado, R.T.A. and F.L. Ferreira (2005) "Measurement of albedo and analysis of its influence in the surface temperature of building roof materials," *Energy and Buildings*, 37 (4), 295-300, doi:10.1016/j.enbuild.2004.03.009.

Rose, L.S. and Levinson, R. (2013) "Analysis of the effect of vegetation on albedo in residential areas: case studies in suburban Sacramento and Los Angeles, CA." *GIScience and Remote Sensing*, 50, 64-77.

Sabins, F. F.(2007) *Remote Sensing – Principles and Interpretation, 3rd ed.* Long Grove, IL: Waveland Press.

Small, C. (2003) "High spatial resolution spectral mixture analysis of urban reflectance," *Remote Sensing of Environment*, 88, 170-186, doi:10.1016/j.rse.2003.04.008.

Taha, H. (1997) "Urban climates and heat islands: albedo, evapotranspiration, and anthropogenic heat," *Energy and Buildings*, 25 (2), 99-103, doi:10.1016/S0378-7788(96)00999-1.

Table 1.

Image and climate characteristics

	PHOENIX	LAS VEGAS
Date	11-Jul-2012	02-Sep-2012
Elevation(m)	*340*	*620*
View angle (°)	6.1	24.3
Sun azimuth (°)	106.9	134.1
Sun angle (°)	62.4	53.1
Air temperature (°C)	39.3	31.7
Dew point temperature (°C)	14.4	1

*at time of satellite overpass. Source http://mesowest.utah.edu

Table 2.

Predicted albedo for the four models, the R^2 of the models, and the error statistics associated with each model

Albedo Range / Reflectance Correction Type	Predicted Albedo at FT*	R^2	Bias	RMS
VNIR / Top-of-Atmosphere	0.226	0.939	-0.097	0.007
VNIR / Surface Reflectance	0.191	0.944	0.27	0.007
Total Shortwave / Top-of-Atmosphere	0.235	0.93	-0.0004	0.008
Total Shortwave / Surface Reflectance	0.207	0.95	0.39	0.007

*** Measured albedo at micrometeorological tower: 0.168**

Table 3.

Models statistical evaluation for the Las Vegas image: the R^2 of the models, and the error statistics associated with the best two models (i.e. surface).

Albedo Range	R^2	Bias	RMS
VNIR	0.928	0.301	0.01
Total Shortwave	0.90	0.46	0.0133

Fig. 1. Location map for the Phoenix, AZ and Las-Vegas, NV study areas. Map on the right indicates the location of Arizona and Nevada within the continental USA.

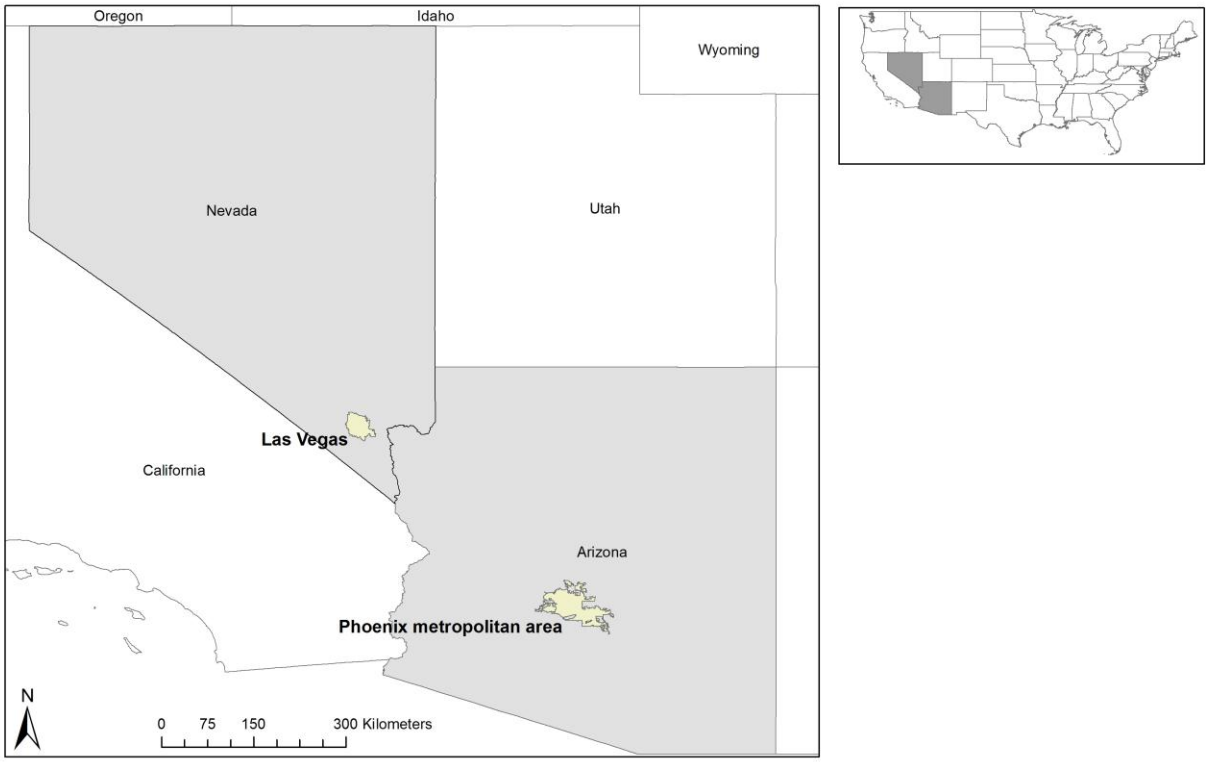

Fig. 2. (a) The QuickBird image used to train the model, overlaid by the field points, the WPHX micrometeorological tower source area, and the MASTER image footprint; (b) the MASTER image; and (c) the WPHX micrometeorological tower and the estimated source area for the installed pyranometer at 22.3 m (73 ft) above surface level. QuickBird bands 4,3 and 2, and MASTER bands 8, 5, and 3 were used for RGB display shown as false-color composites for the three images.

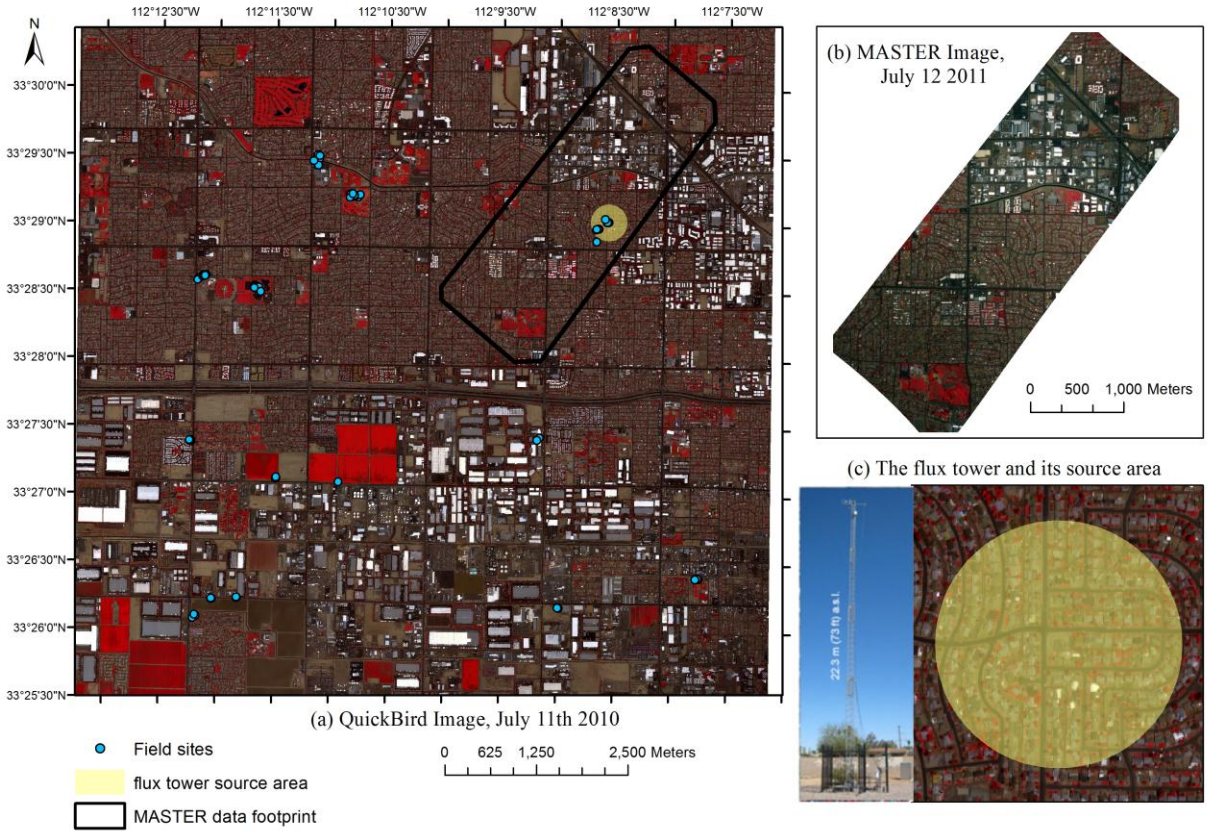

Fig. 3. Spectral signatures of dominant land cover in the PHX region. Gaps correspond to water absorption bands.

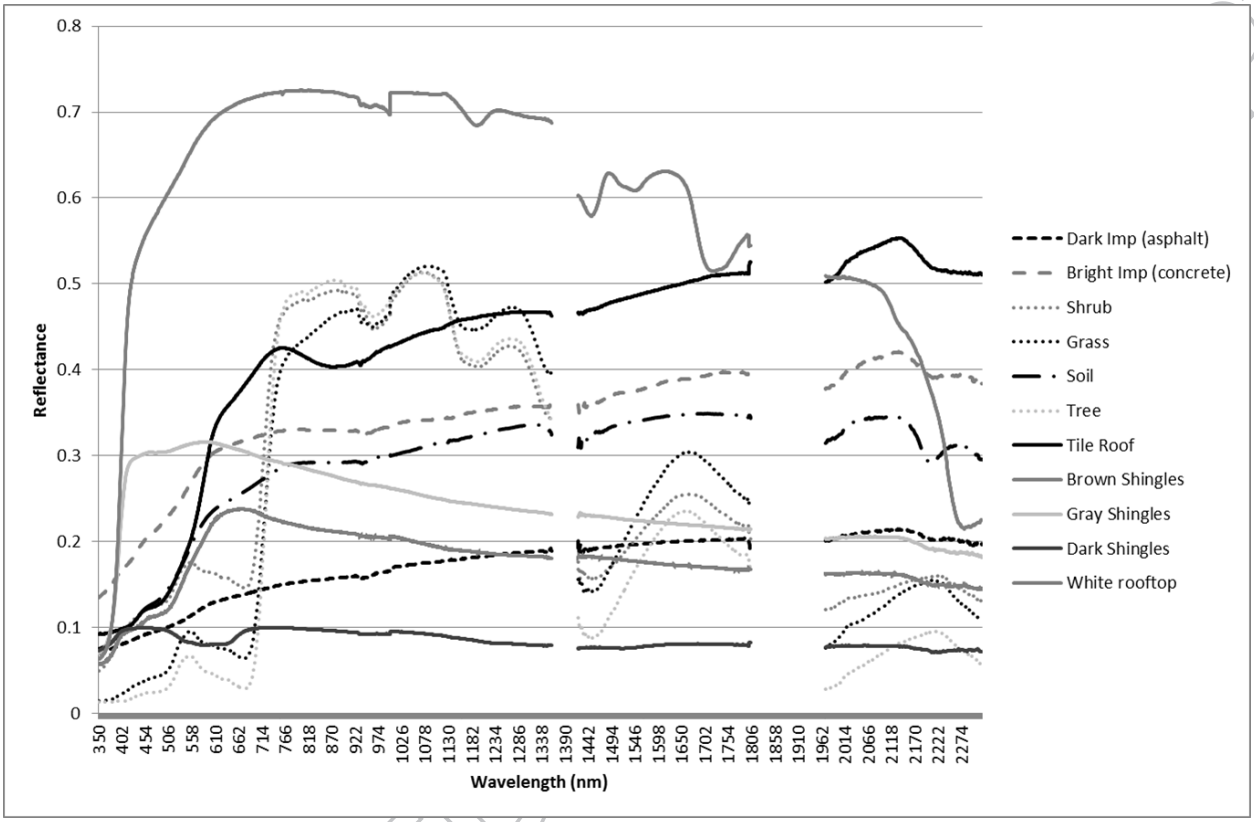

Fig. 4. Comparison between atmospherically corrected image reflectance and ground spectra. Symbols represent different land covers, while colors correspond to the four QuickBird bands, i.e – Blue (450-520nm), Green (520-600nm), Red (630-690nm) and NIR (760-900nm).

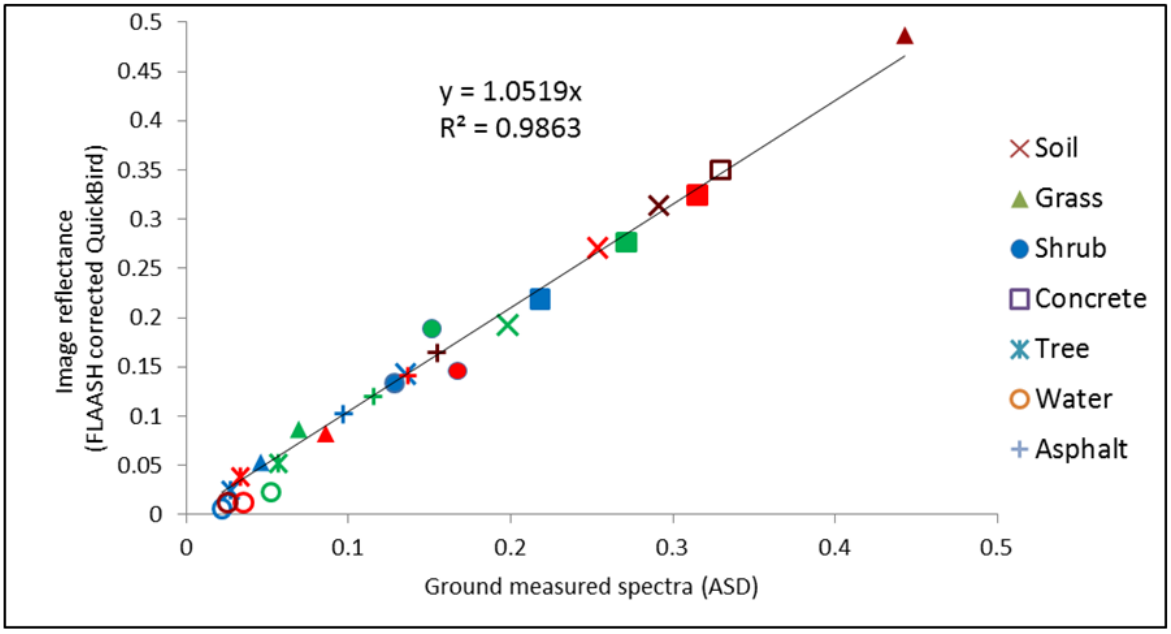

Fig. 5. Broadband albedo maps of the Phoenix study area, using the TOA/VNIR model (a) and TOT/Surf (b).

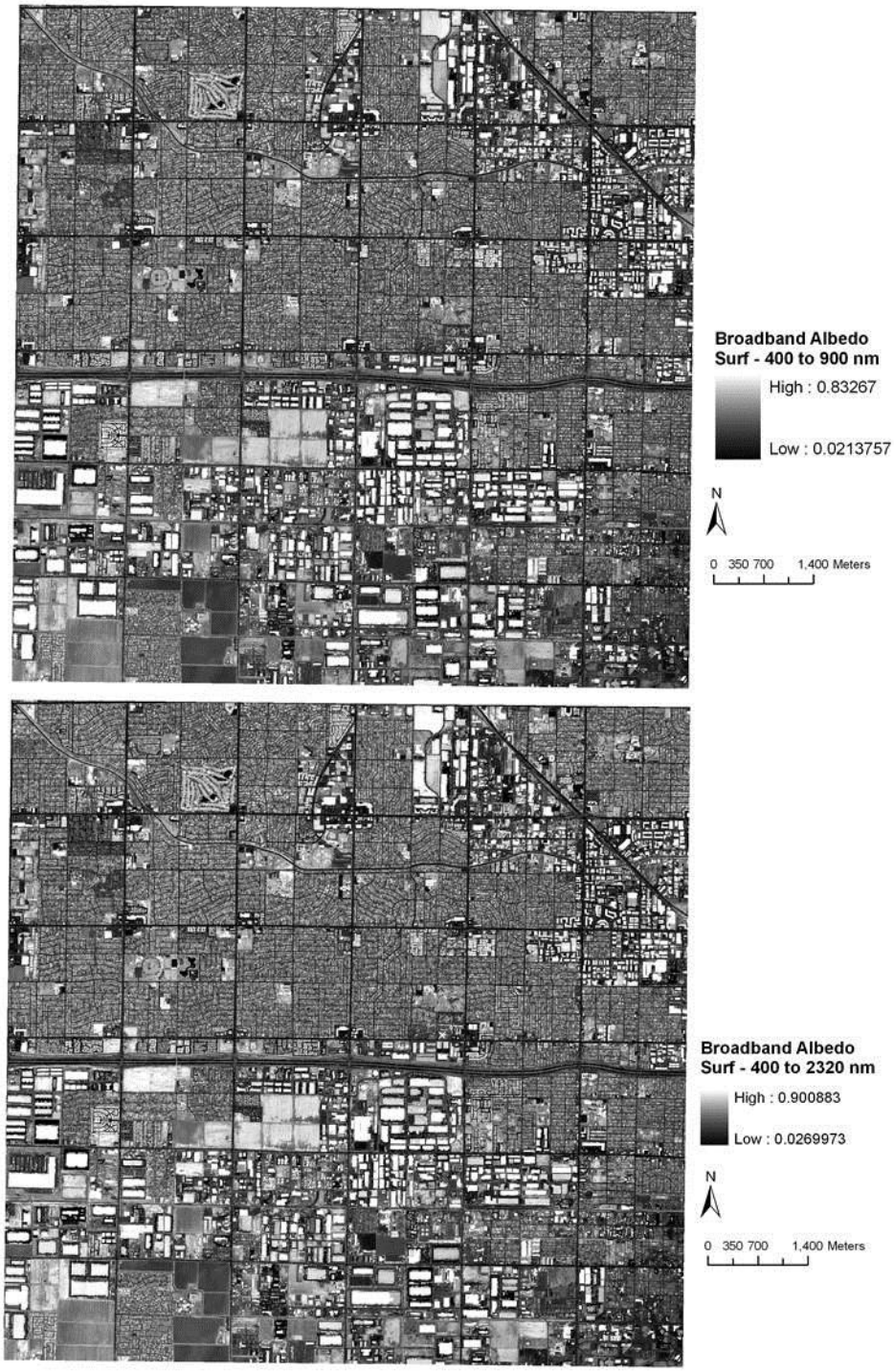

Fig. 6. Relationship between ground-measured albedo and the predicted albedo for the four models: (a) VNIR-TOA, (b) TOT-TOA, (c)VNIR-SURF, (d) TOT-SURF.

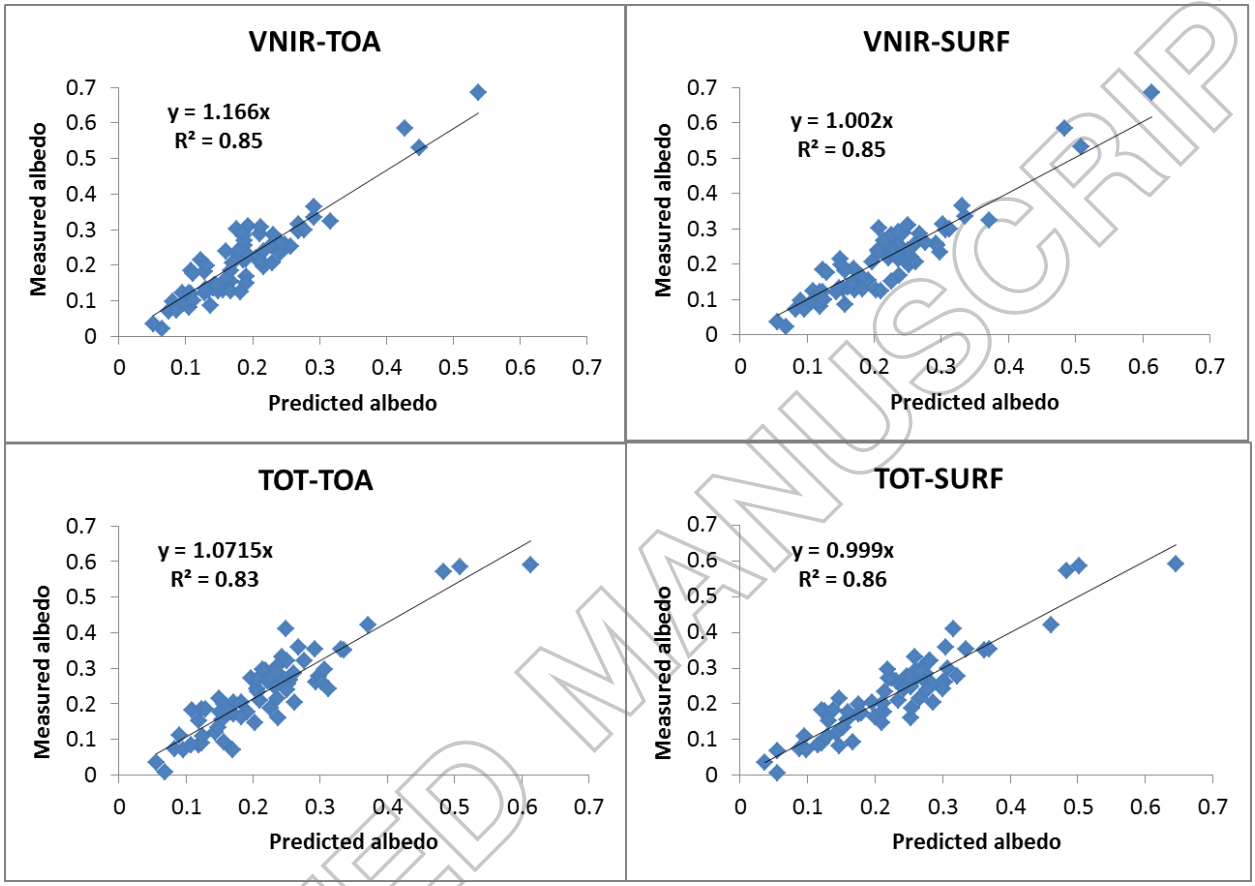

Fig. 7. Relationship between albedo estimates from MASTER and the predicted albedo from the VNIS/Surface model.

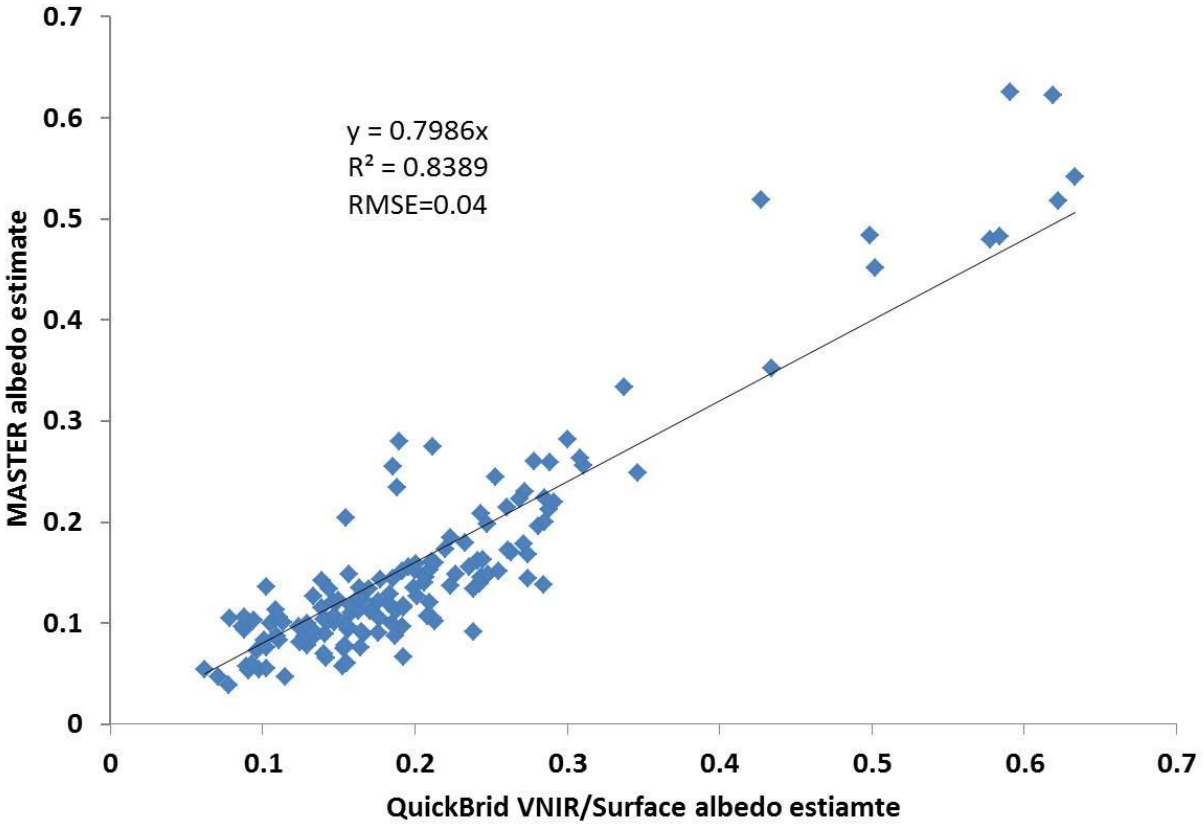

Fig. 8. QuickBird image of the Las Vegas study area with field points (top) and the broadband albedo map using the VNIR/Surf model (bottom).